

Finite-time quantum Otto engine: Surpassing the quasi-static efficiency due to friction

Sangyun Lee,¹ Meesoon Ha,^{2,*} Jong-Min Park,³ and Hawoong Jeong^{4,†}

¹*Department of Physics, Korea Advanced Institute of Science and Technology, Daejeon 34051, Korea*

²*Department of Physics Education, Chosun University, Gwangju 61452, Korea*

³*School of Physics, Korea Institute for Advanced Study, Seoul, 02455, Korea*

⁴*Department of Physics and Institute for the BioCentury,*

Korea Advanced Institute of Science and Technology, Daejeon 34141, Korea

(Dated: June 14, 2022)

In finite-time quantum heat engines, some work is consumed to drive a working fluid accompanying coherence, which is called ‘friction’. To understand the role of friction in quantum thermodynamics, we present a couple of finite-time quantum Otto cycles with two different baths: Agarwal versus Lindbladian. We exactly solve them and compare the performance of the Agarwal engine with that of the Lindbladian one. Particularly, we find remarkable and counterintuitive results that the performance of the Agarwal engine due to friction can be much higher than that in the quasi-static limit with the Otto efficiency, and the power of the Lindbladian engine can be non-zero in the short-time limit. Based on additional numerical calculations of these outcomes, we discuss possible origins of such differences between two engines and reveal them. Our results imply that even with equilibrium bath, a non-equilibrium working fluid brings on the higher performance than what an equilibrium one does.

I. INTRODUCTION

How quantumness plays a role in thermodynamics is one of interesting and important questions to understand quantum phenomena, which is so-called *quantum thermodynamics* [1] that concerns the relation between quantum mechanics and thermodynamics. In a sense, to study quantum heat engines [2] (and references therein) has provided useful frameworks for further theoretical and experimental developments.

A quantum heat engine is a cycle with thermodynamic processes, and its working fluid is a quantum system with coherence, entanglement, and discrete energy levels. Due to the development of experimental techniques, it has been realized in various ways [3–5], and various heat baths have been also considered: Coherent bath was used to exceed the Carnot efficiency, and decoherent one was introduced to find the signature of quantumness [6–8]. Squeezed bath [9] also allowed the efficiency to be beyond the Carnot efficiency due to the nonequilibrium resource. Moreover, it is known that quantum phase transition can be used to increase the efficiency [10] or decrease it [11].

Owing to the discovery of the trade-off relation between the power and the efficiency of the engine [12, 13] as well as the development of the shortcut-to-adiabaticity technique [14], the finite-time quantum heat engine has steadily gathered many attentions, where the working fluid can have coherence without any special bath, such as a squeezed or coherent bath. When Hamiltonians at different times do not commute, a portion of work is used to generate coherence, which is dissipated when the system is coupled to a heat bath later.

Such a mechanism is regarded a quantum analogue of *friction*. There have been many ways to measure friction in quantum heat engines [15–18], but we focus only on the friction by the power term that is required to drive the working fluid in the finite-time mode, which has been in Otto heat engines [15, 16].

The Otto cycle (see Fig. 1) has been widely studied due to its analytic tractability [11, 14–16, 19–23]. Its experimental realizations reported that it can be used as a precise thermometer [24], and its quasi-static efficiency can be beaten in finite time with a heat bath of effective negative temperatures [5]. In addition, recent shortcut-

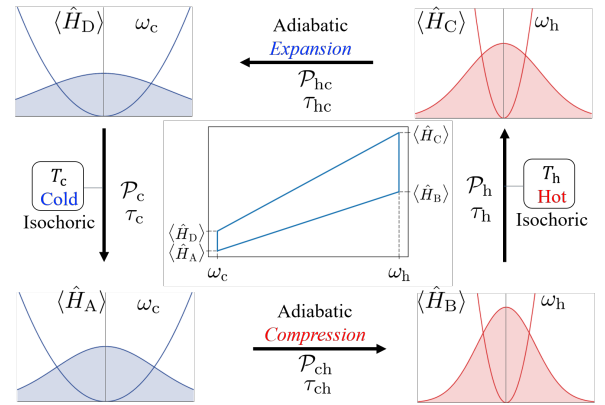


FIG. 1. A finite-time quantum Otto cycle is schematically illustrated with harmonic potentials and Wigner functions, which consists of isochoric and adiabatic processes. In the isochore, the working fluid exchanges heat with heat bath of temperature $T_{h/c}$ by the propagator, $\mathcal{P}_{h/c}$, of the vector, $(\langle \hat{H} \rangle, \langle \hat{L} \rangle, \langle \hat{D} \rangle, \langle \hat{I} \rangle)$ for the process time $\tau_{h/c}$, whereas, in the adiabatic expansion/compression, the internal energy change of the working fluid becomes work by $\mathcal{P}_{hc/ch}$ for $\tau_{hc/ch}$. The total energy expectation of the working fluid is drawn as a function of ω in the middle panel.

* msha@chosun.ac.kr

† hjeong@kaist.edu

to-adiabaticity technique application about Otto engine focus engine with Otto efficiency and non-zero power [14].

In this paper, we consider two quantum Otto cycles in finite-time frameworks with a time-dependent harmonic oscillator, exactly solve their performances, and discuss the role of friction in them as its quantum effect. To describe a quantum system connecting to the corresponding heat bath, we revisit the well-known Lindblad master equation (Lindblad bath, **L**) [25] with a propagator of a dynamical semigroup, and the Agarwal master equation (Agarwal bath, **A**) [26, 27] (and references therein) as paradigmatic models. In particular, we focus on how they are different from each other in the finite-time mode. Finally, it turns out that they exhibit fruitful physics with remarkable and counterintuitive results.

In the quasi-static limit, regardless of detailed model approaches, the Otto efficiency is only determined by the volume ratio between hot and cold isochores. As the cycle time becomes infinity, its power becomes eventually zero. As a result, the quasi-static limiting performance of quantum Otto heat engines is rather trivial, so that two baths (propagators) do not make any difference between their performances in the quasi-static limit. However, in the finite-time mode, they can be different due to the role of friction and the setup of heat bath. To our best knowledge, the case of the Lindblad bath was exactly solved, but the Agarwal case has not been exactly solved yet. So, in this paper, we exactly solve the Agarwal case and compare it to the Lindbladian, and address how we can improve the performance of the finite-time quantum Otto cycle. Our remarkable and counterintuitive results can be used for the possibility of engineering friction term to improve the performance of the quantum heat engine.

The rest of this paper is organized as follows. In Sec. II, we describe a finite-time quantum Otto heat engine with harmonic oscillator and present two different types of baths, where the performances (efficiency and power) of Otto cycles are denoted with the analytic forms of work and heat. In Sec. III, we exactly solve the performance of each case as well as numerical enumerations for related physical quantities, where we argue the possible origins of the differences between two cases and confirm them. In particular, we focus on the performance in the short-time limit and near the resonance conditions, where the performance of the engine is improved counterintuitively. Finally, in Sec. IV, we conclude this paper with summary and some remarks.

II. SYSTEM

A. Otto cycle

As illustrated in Fig. 1, an Otto cycle consists of two isochoric (constant volume) and two adiabatic (no heat transfer) processes. In the isochore, there is no external force and no explicit time dependence on Hamiltonian, $\hat{H}(t)$, so that all the energy change of the engine be-

comes heat. We consider a couple of heat baths for the isochores, which drive a system into the same equilibrium state, the Lindblad bath versus the Agarwal bath.

The governing equation of the density matrix is

$$\frac{d\hat{\rho}(t)}{dt} = -\frac{i}{\hbar}[\hat{H}(t), \hat{\rho}(t)] + \mathcal{L}_k(\hat{\rho}(t)). \quad (1)$$

where \mathcal{L}_k is a superoperator to describe an interaction between the working fluid and heat bath, and k is either **A** (Agarwal) or **L** (Lindbladian). Equation (1) without the superoperator is just a von Neumann equation, which describes a close quantum system. It is noted that a hat symbol ($\hat{\cdot}$) denotes operator.

The superoperator of Agarwal bath [27] is written as

$$\mathcal{L}_A(\hat{\rho}(t)) = -\frac{i\kappa}{\hbar}[\hat{x}, \{\hat{p}, \hat{\rho}(t)\}] - \frac{2\kappa m\omega}{\hbar}(\bar{n} + \frac{1}{2})[\hat{x}, [\hat{x}, \hat{\rho}(t)]]. \quad (2)$$

where κ is a heat conductance that governs the energy exchange rate between the working fluid and the Agarwal bath, and \bar{n} is the expectation value of the number operator for the heat bath of temperature T ($\bar{n} = [\exp(\hbar\omega/k_B T) - 1]^{-1}$). Expanding Eq. (2) in the high-temperature limit, it becomes the Caldeira-Leggett master equation, which is well-known to model quantum tunneling phenomena in a dissipative system [28].

For the Lindblad bath, it is as follows:

$$\begin{aligned} \mathcal{L}_L(\hat{\rho}(t)) = & \frac{\gamma}{2}(\bar{n} + 1)[\hat{a}\hat{\rho}(t)\hat{a}^\dagger - \frac{1}{2}(\hat{a}^\dagger\hat{a}\hat{\rho}(t) + \hat{\rho}(t)\hat{a}^\dagger\hat{a})] \\ & + \frac{\gamma}{2}\bar{n}[\hat{a}^\dagger\hat{\rho}(t)\hat{a} - \frac{1}{2}(\hat{a}\hat{a}^\dagger\hat{\rho}(t) + \hat{\rho}(t)\hat{a}\hat{a}^\dagger)], \end{aligned} \quad (3)$$

where γ is heat conductance of the Lindblad bath [29] and \hat{a} (\hat{a}^\dagger) represents an annihilation (creation) operator. The annihilation operator is the combination of position and momentum operators, $\hat{a} = \sqrt{\frac{m\omega}{2\hbar}}(\hat{x} + \frac{i}{m\omega}\hat{p})$, and the creation operator is the complex conjugate of \hat{a} , $\hat{a}^\dagger = \sqrt{\frac{m\omega}{2\hbar}}(\hat{x} - \frac{i}{m\omega}\hat{p})$. For the adequate comparison of the Agarwal bath with the Lindblad bath, we set the heat conductance of the Agarwal bath as $\kappa = \gamma/8$.

In the adiabatic process, the volume of the working fluid is changed without heat transfer between heat bath and the working fluid, so that the master equation with $\gamma = 0$ corresponds to the adiabatic process, where $\hat{H}(t)$ is explicitly time-dependent and all the energy change of the working fluid becomes work.

Combining these processes into a quantum Otto cycle, we generate the following procedure: First, we compress the working fluid in the adiabatic process, where work is exerted on the working fluid and its energy level becomes higher than that before it was. Second, we connect the working fluid to a hot bath with temperature T_h . In the hot isochore, heat is transferred to the working fluid from the hot bath, which is transformed as other types in the following adiabatic process. Third, in the adiabatic process, we expand the working fluid, so that the energy

of the engine is transferred to the external agent. Finally, in the cold isochore, we connect the working fluid to the cold bath with temperature T_c . Since the working fluid does not connect to the heat bath when Hamiltonian has the explicit time dependence, solving an Otto engine is easier than other finite-time cyclic heat engines.

B. Working fluid: Harmonic oscillator

To make our problem simple and analytical tractable, we employ harmonic oscillators as the working fluid of the Otto cycle. The harmonic oscillator is useful to model diverse phenomena, such as a cavity, a trapped ion, a RLC circuit, and a mechanical spring. The Hamiltonian for the time-dependent harmonic oscillator is given by

$$\hat{H}(t) = \frac{\hat{p}^2}{2m} + \frac{m\omega^2(t)\hat{x}^2}{2}, \quad (4)$$

where m and \hat{x} (\hat{p}) are mass and position (momentum) operator, respectively. For the harmonic gas, it is known that the inverse of the frequency $\omega(t)$ corresponds to the volume of the working fluid [30]. Hence, in the adiabatic process, we change the frequency $\omega(t)$, whereas in the isochore, we do not.

With the Wigner function representation, we can map Eq. (1) for the density matrix to an equation for the c -number. The Wigner function describes a quasi-probability that represents the density function operator as a real function, which is written as

$$W(x, p) = \frac{1}{\pi\hbar} \int dz e^{-2ipz/\hbar} \langle x + z | \hat{\rho}(t) | x - z \rangle. \quad (5)$$

The quasi-probability does not satisfy probability axioms and can have negative values. For the Gaussian state, $W(x, p)$ is guaranteed to be non-negative value [31].

For the harmonic oscillator, the master equation of $W(x, p)$ is

$$\partial_t W(x, p) = -\vec{\nabla}_q \cdot [\mathcal{A}_k \cdot \vec{q} - \mathcal{B}_k \cdot \vec{\nabla}_q] W(x, p), \quad (6)$$

where

$$\mathcal{A}_A = \begin{pmatrix} 0 & \frac{1}{m} \\ -m\omega^2(t) & -\frac{\gamma}{4} \end{pmatrix}; \quad \mathcal{B}_A = \begin{pmatrix} 0 & 0 \\ 0 & \frac{m\gamma}{4} \tilde{T} \end{pmatrix} \quad (7)$$

for the Agarwal bath, and

$$\mathcal{A}_L = \begin{pmatrix} -\frac{\gamma}{4} & \frac{1}{m} \\ -m\omega^2(t) & -\frac{\gamma}{4} \end{pmatrix}; \quad \mathcal{B}_L = \begin{pmatrix} \frac{\gamma\tilde{T}}{4m\omega^2(t)} & 0 \\ 0 & \frac{m\gamma\tilde{T}}{4} \end{pmatrix} \quad (8)$$

for the Lindblad bath, and $\tilde{T} = \hbar\omega(\bar{n} + 1/2)$.

Equation (6) has the same structure of the Fokker-Planck equation [32]. The corresponding Langevin equation to the master equation of the Wigner function is called the quasi-classical Langevin equation [31]. The Langevin equation for the Agarwal bath is

$$\begin{aligned} \partial_t x &= \frac{p}{m}, \\ \partial_t p &= -m\omega^2 x - \frac{\gamma}{4} p + \sqrt{\frac{\gamma\hbar m\omega(\bar{n} + 1/2)}{4}} \eta_p(t), \end{aligned} \quad (9)$$

where $\langle \eta_i(t)\eta_j(t') \rangle = 2\delta_{i,j}\delta(t-t')$. In this case, if we take the high temperature limit, then Eq. (9) becomes the Langevin equations for a Brownian particle.

The Langevin equations for the Lindblad bath are

$$\begin{aligned} \partial_t x &= \frac{p}{m} - \frac{\gamma}{4} x + \sqrt{\frac{\gamma\hbar(\bar{n} + 1/2)}{4m\omega}} \eta_x(t), \\ \partial_t p &= -m\omega^2 x - \frac{\gamma}{4} p + \sqrt{\frac{\gamma\hbar m\omega(\bar{n} + 1/2)}{4}} \eta_p(t). \end{aligned} \quad (10)$$

It is noted that, for the Lindblad bath, an additional heat channel exists in position. For the governing equation for momentum, both cases are exactly the same due to the choice of $\kappa = \gamma/8$, which helps to resolve the role of the positional heat channel in Eq. (9). Due to this fact, the relaxation of potential energy for the Lindblad bath and the Agarwal bath are quite different, which leads to huge difference in the performances of both Otto engines in finite time. Such outcomes are presented and discussed with possible origins in Sec. III.

Since Eq. (6) has the quadratic form, the cyclic steady state of Otto engines can be described by Gaussian. As a result, the Wigner function is non-negative in limit cycle [33]. Due to the left-right symmetry for the breathing potential, $\langle \hat{x} \rangle$ and $\langle \hat{p} \rangle$ are zero in cyclic steady state. Therefore, it is enough to calculate the second moments for describing cyclic steady states.

With the adjoint master equation of $W(x, p)$, we can write down equations for Hamiltonian \hat{H} , Lagrangian \hat{L} , and a correlation function \hat{D} , respectively:

$$\begin{aligned} \hat{H}(t) &= \hat{p}^2/2m + m\omega^2(t)\hat{x}^2/2, \\ \hat{L}(t) &= \frac{\hat{p}^2}{2m} - \frac{m\omega^2(t)\hat{x}^2}{2}, \\ \hat{D}(t) &\equiv \omega(t)(\hat{x}\hat{p} + \hat{p}\hat{x})/2, \end{aligned}$$

which are the linear combinations of second moments.

The evolution of a vector

$$\vec{\phi}(t) \equiv (\langle \hat{H}(t) \rangle, \langle \hat{L}(t) \rangle, \langle \hat{D}(t) \rangle, \langle \hat{I} \rangle)^T$$

where \hat{I} is an identity operator. The vector is governed by a linear master equation [16]:

$$\frac{d}{dt} \vec{\phi}(t) = \mathcal{M}_j^k \vec{\phi}(t), \quad (11)$$

where k is either **A** or **L**, and j is either adiabatic (**a**) or isochoric (**i** in $\{c, h\}$).

In the adiabatic process, the matrix \mathcal{M} of Eq. (11) is written as

$$\mathcal{M}_a^{A/L} = \omega(t) \begin{pmatrix} \frac{\dot{\omega}(t)}{\omega^2(t)} & -\frac{\dot{\omega}(t)}{\omega^2(t)} & 0 & 0 \\ -\frac{\dot{\omega}(t)}{\omega^2(t)} & \frac{\dot{\omega}(t)}{\omega^2(t)} & -2 & 0 \\ 0 & 2 & \frac{\dot{\omega}(t)}{\omega^2(t)} & 0 \\ 0 & 0 & 0 & 0 \end{pmatrix}. \quad (12)$$

Here work per time is given as

$$\partial_t \langle \hat{H} \rangle = \frac{\dot{\omega}(t)}{\omega(t)} (\langle \hat{H} \rangle - \langle \hat{L} \rangle). \quad (13)$$

In the right-hand side of Eq. (13), the second term associated with $\langle \hat{L} \rangle$ is called *friction* because it disappears in the quasi-static limit and decreases the power of Otto heat engines in the finite-time mode [16]. However, we will show that in the engine with Agarwal bath, the friction term can have the same sign as the first term, so that it helps to enhance the performance of the engine.

When $\dot{\omega}(t)/\omega^2(t)$ is constant, we can factor out $\omega(t)$ in the adiabatic matrix \mathcal{M}_a and the solution of Eq. (11) has a closed form [34].

$$\omega(t) = \frac{\omega_i \omega_f}{\omega_f \tau - (\omega_f - \omega_i)t}, \quad (14)$$

where i is initial, f is final, and τ is the time of the adiabatic process. Then the propagator of the adiabatic process, \mathcal{P}_{if} , is written as

$$\ln(\mathcal{P}_{if}) = \begin{pmatrix} r_w & -r_w & 0 & 0 \\ -r_w & r_w & \frac{2\tau_{if} r_w}{\omega_f^{-1} - \omega_i^{-1}} & 0 \\ 0 & -\frac{2\tau_{if} r_w}{\omega_f^{-1} - \omega_i^{-1}} & r_w & 0 \\ 0 & 0 & 0 & 0 \end{pmatrix}, \quad (15)$$

where $r_w \equiv \ln(\omega_f/\omega_i)$. For the simplicity, we take the notation of the propagator of the adiabatic compression (expansion) process as \mathcal{P}_{ch} (\mathcal{P}_{hc}) as stated in Fig. 1.

In the isochore, the matrix \mathcal{M} of Eq. (11) is given as

$$\mathcal{M}_i^A = \begin{pmatrix} -\frac{\gamma}{4} & -\frac{\gamma}{4} & 0 & \frac{\gamma \tilde{T}_i}{4} \\ -\frac{\gamma}{4} & -\frac{\gamma}{4} & -2\omega_i & \frac{\gamma \tilde{T}_i}{4} \\ 0 & 2\omega_i & -\frac{\gamma}{4} & 0 \\ 0 & 0 & 0 & 0 \end{pmatrix} \quad (16)$$

and

$$\mathcal{M}_i^L = \begin{pmatrix} -\frac{\gamma}{2} & 0 & 0 & \frac{\gamma \tilde{T}_i}{2} \\ 0 & -\frac{\gamma}{2} & -2\omega_i & 0 \\ 0 & 2\omega_i & -\frac{\gamma}{2} & 0 \\ 0 & 0 & 0 & 0 \end{pmatrix} \quad (17)$$

where \mathbf{i} is h (c) for the hot (cold) isochore. Because the matrix in the isochore is independent of time, the propagator is given as $\mathcal{P}_i^k = \exp(\mathcal{M}_i^k t)$. By substituting the matrix in Eq. (11) with Eq. (16) and Eq. (17), equations for evolution of Hamiltonian, Lagrangian and correlation is earned. For the case of \mathcal{M}_i^L , $\langle \hat{H} \rangle$ directly approaches to energy in equilibrium and does not couple to $\langle \hat{L} \rangle$ and $\langle \hat{D} \rangle$. On the other hand, for the case of \mathcal{M}_i^A , they are coupled to one another. This difference leads to a big difference of the performances of finite-time engines in cyclic steady states, which is shown in Sec. III in detail.

Rearranging equations for the isochores, we obtain the equations for potential energy (PE) and kinetic energy

(KE), respectively. The dynamic equations of PE and KE are written as

$$\begin{aligned} \frac{d}{dt} \langle \frac{\hat{p}^2}{2m} \rangle &= -\frac{\gamma}{2} \langle \frac{\hat{p}^2}{2m} \rangle - \omega_i D + \frac{\gamma \tilde{T}_i}{4}, \\ \frac{d}{dt} \langle \frac{m\omega_i^2 \hat{x}^2}{2} \rangle &= \omega_i D. \end{aligned} \quad (18)$$

for the Agarwal bath and

$$\begin{aligned} \frac{d}{dt} \langle \frac{\hat{p}^2}{2m} \rangle &= -\frac{\gamma}{2} \langle \frac{\hat{p}^2}{2m} \rangle - \omega_i D + \frac{\gamma \tilde{T}_i}{4}, \\ \frac{d}{dt} \langle \frac{m\omega_i^2 \hat{x}^2}{2} \rangle &= \omega_i D - \frac{\gamma}{2} \langle \frac{m\omega_{bf}^2 \hat{x}^2}{2} \rangle + \frac{\gamma \tilde{T}_i}{4}. \end{aligned} \quad (19)$$

for the Lindblad bath. For both cases, the governing equation for KE is the same and this is our criterion to regulate a heat conductance for both baths. From propagator expressions as shown in Fig. 1, we are able to calculate cyclic steady states and the performance of engines regarding the assigned bath. The propagator for one cycle is given by $\mathcal{P}_{cyc}^k \equiv \mathcal{P}_c^k \mathcal{P}_{hc}^k \mathcal{P}_h^k \mathcal{P}_{ch}^k$.

With the condition that Hamiltonian, Lagrangian and the correlation function remain the same after one cycle, the cyclic steady state $\vec{\phi}_{ss}^k$ can be calculated [34]. Then, work and heat are written as

$$\begin{aligned} \mathcal{W}_{ch}^k &= \vec{d} \cdot (\mathcal{P}_{ch} - \mathcal{I}) \cdot \vec{\phi}_{ss}^k \\ \mathcal{W}_{hc}^k &= \vec{d} \cdot (\mathcal{P}_{hc} - \mathcal{I}) \mathcal{P}_h^k \mathcal{P}_{ch}^k \cdot \vec{\phi}_{ss}^k \\ Q_h^k &= \vec{d} \cdot (\mathcal{P}_h^k - \mathcal{I}) \mathcal{P}_{ch}^k \cdot \vec{\phi}_{ss}^k \\ Q_c^k &= \vec{d} \cdot (\mathcal{P}_c^k - \mathcal{I}) \mathcal{P}_{hc}^k \mathcal{P}_h^k \mathcal{P}_{ch}^k \cdot \vec{\phi}_{ss}^k, \end{aligned} \quad (20)$$

where

$$\vec{d} \equiv (1, 0, 0, 0)^T \quad (21)$$

and \mathcal{I} is an identity matrix of size four. From Eq. (20), the performance of the Otto engine, its efficiency and power, can be calculated as follows:

$$\begin{aligned} \eta^k &= -(\mathcal{W}_{ch}^k + \mathcal{W}_{hc}^k)/Q_h^k, \\ P^k &= -(\mathcal{W}_{ch}^k + \mathcal{W}_{hc}^k)/\tau_{cyc}. \end{aligned} \quad (22)$$

III. RESULTS

In this section, we present the remarkable difference between Agarwal and Lindbladian Otto engines, in the context of the performance of the finite-time engine, which is based on exact solutions. However, the exact mathematical forms are not directly shown in this paper since they are quite complicated. Instead, we present the analytic forms of the approximated result in the short cycle-time limit. Using the analytic condition for the divergence of the engine with the resonance, we show that the finite-time Otto heat engine is different from the quasi-static limiting case. For the finite-time performance, we provide enumerated results to support our

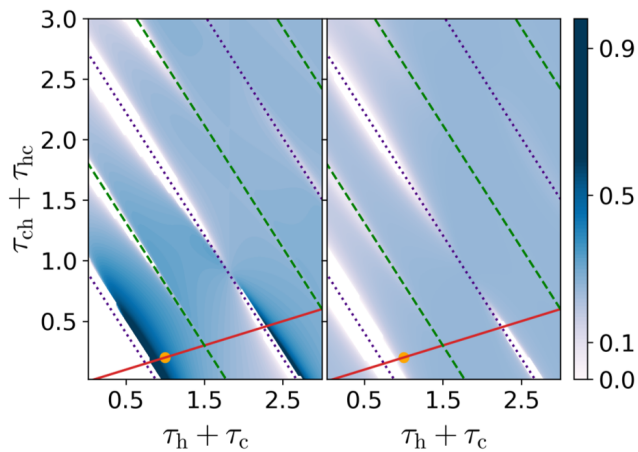


FIG. 2. The contour plots of η^A (left) and η^L (right) are presented as a function of $\tau_h + \tau_c$ (the sum of the isochoric time, x-axis) and $\tau_{ch} + \tau_{hc}$ (the sum of the adiabatic time, y-axis). Since we plot only when the cycle behaves as a heat engine, there are diagonal white lines. Unless isochoric process time is long, the white lines well coincides with purple dotted (green dashed) lines which are derived from Eq. (24) when n is odd (even). Near purple resonance lines, we can find some regions that show $\eta^A \gg \eta^L$. In both panels, the red solid line represents $(\tau_{ch} + \tau_{hc})/(\tau_h + \tau_c) = 1/5$, and the orange dot corresponds to the case of $\tau_{cyc} = 1.2$, which is discussed in Fig. 3 and Fig. 4. Here we set all parameters to be dimensionless and $\hbar = k_B = m = \gamma = 1$, $\omega_h = 4, \omega_c = 3, T_h = 200$, and $T_c = 1$, which are kept used from now on unless other values are indicated separately. For the simplicity, we choose $\tau_h = \tau_c$ and $\tau_{ch} = \tau_{hc}$.

interesting findings, where we set all the parameters to be dimensionless, and for the simplicity, $k_B = \hbar = 1$.

Before moving onto our results, we briefly review the quasistatic behavior and give some intuition of the Otto heat engine. When the time periods of both adiabatic processes are sufficiently large, the engine has the universal efficiency, $\eta_O = 1 - \omega_c/\omega_h$, known as the quantum Otto efficiency [16]. The Otto efficiency is smaller than the Carnot efficiency $\eta_C = 1 - T_c/T_h$. This statement is consistent with the fact that the system operates as an engine only when $T_c/T_h > \omega_c/\omega_h$. In the quasi-static limit, if we control the frequency ratio beyond it, the Otto cycle becomes a refrigerator, rather than a heat engine.

In Fig. 2, we show how the Agarwal (Lindbladian) Otto engine in the left (right) panel works with the following parameter settings: $m = \gamma = 1, \omega_h = 4, \omega_c = 3, T_h = 200$, and $T_c = 1$. The x-axis (y-axis) is the sum of two isochoric (adiabatic) times, and we plot the efficiency only when the engine behaves as heat engine. Due to the divergence/resonance condition (23), there is a white stripes. The Otto engine with the harmonic oscillator shows resonant behaviors because position determines how a force is exerted on a particle. When the phase difference per cycle is a multiple of π , the energy of the cycle can be stored indefinitely to the particle. For the Otto heat engine, the resonance condition is calculated

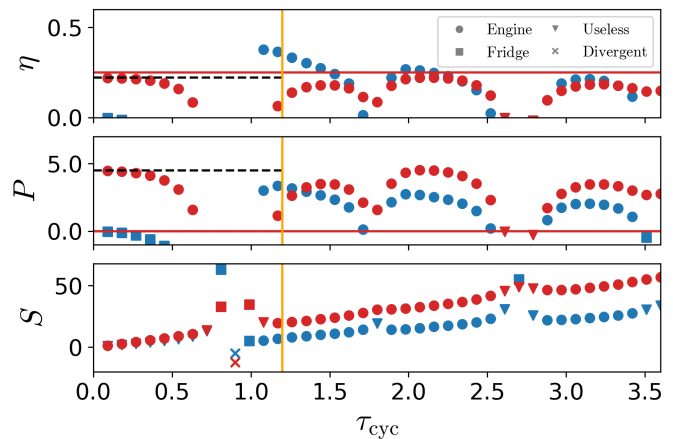


FIG. 3. Along the red line of each panel in Fig. 2, we compare the performance of Agarwal Otto engine (blue, \bullet) with that of Lindbladian (red, \bullet), in the context of its efficiency η (top), power P (middle), and entropy S (bottom), which are as a function of τ_{cyc} . In the quasi-static limit ($\tau_{cyc} \rightarrow \infty$), $\eta^A/\eta^L \rightarrow \eta_O$ and $P^A/\eta^L \rightarrow 0$, which are drawn as horizontal red solid lines. In addition, the analytic short-time results of Eq. (25) for η^L and P^L are drawn as horizontal black dashed lines up to $\tau_{cyc} = 1.2$, whereas $\eta^A \rightarrow 0$ and $P^A \rightarrow 0$. Vertical orange solid lines are drawn at $\tau_{cyc} = 1.2$ (orange dots in Fig. 2), where $\eta^A > \eta_O > \eta^L$. For non-engine or unphysical values, we use different symbols from that of the heat engine and put some explanations as keys: fridge, useless, and divergent.

as follows:

$$n\pi = \int_0^{\tau_{cyc}} dt \omega(t) \quad (23)$$

The simplified resonance condition can be written as

$$n\pi = \omega_c \tau_c + \omega_h \tau_h + \frac{\omega_c \omega_h}{\omega_h - \omega_c} \ln(\omega_h/\omega_c)(\tau_{ch} + \tau_{hc}). \quad (24)$$

The right hand side of Eq. (24) is the summation of phase difference for the four processes in the Otto cycle. Near the condition of Eq. (24) in the short-time region, the working fluid continuously gets energy, so that energy diverges. However, if the contact time with heat bath is long enough to be dissipated, then energy does not pile up in the working fluid.

In Fig. 3, we show the performance of two finite-time Otto engines along the red line of each panel in Fig. 2, where the ratio of a isochoric time to an adiabatic time is fixed as 5 : 1. The finite-time quantum Otto cycle can be one of the following four ways: In the heat engine, heat flow is converted to work. In the refrigerator, heat is absorbed from cold bath due to work. In the useless machines, both work and heat are consumed and exert into cold bath. We allocate different symbols to each case, circles for engines, squares to refrigerators, triangles to useless machines, and crosses to divergent case in Fig. 3. We also present the behavior of the entropy for both cases, which show that the entropy in the short-time

limit is the same, but the Lindbladian case is larger than the Agarwal case in the finite-time mode.

A noticeable difference between the Agarwal Otto engine and the Lindbladian one is that the efficiency of the Agarwal case is higher than that of the Lindbladian case near the resonant condition from Eq. (24). Particularly, when the phase difference of the cycle is the odd multiples of π , the high efficiency is observed, which is even higher than the Otto efficiency in the quasi-static limit.

This can be briefly explained by the classical scheme: The working fluid oscillates with $\omega(t)$. If the distance between the particle and the center of the potential is large in the adiabatic process, the large amount of energy is extracted or absorbed to/from the external agent. Suppose that the phase difference for each process is $(n/4)\pi$, there is a phase difference, $(n/2)\pi$ between adiabatic compression and adiabatic expansion processes. With the even number of n , even though we extract much energy from the working fluid in the adiabatic compression process, we also spend much energy. With the odd number of n , the engine can spend small energy to compress and extract large energy, so that the high efficiency can be observed only near the odd phase difference condition.

However, the explanation of the resonance condition does not fully explain why there is a difference between two engines. To figure out the origin of such a notable difference, we measure trajectories KE and PE of the limit cycle at $\tau_{\text{cyc}} = 1.2$ when the difference is dominant. It is because they are essential to calculate the expectation values of Hamiltonian and Lagrangian.

In Fig. 4, we present the expectation values of KE and PE for each engine at $\tau_{\text{cyc}} = 1.2$ (orange vertical line in Fig. 3), where the solid (dashed) line are PE (KE). It is observed that for the Agarwal Otto engine (red), the PE is always larger than the KE in the adiabatic expansion process ($0.6 \leq t \leq 0.7$). This means that the friction term, the second term of Eq. (13), has the same sign as that of Hamiltonian. As a result, the friction term improves the efficiency of finite-time Agarwal Otto engine to exceed η_{O} . It is noted that in the quasi-static limit, the friction term becomes zero. Contrast of the imbalance between KE and PE in expansion process is originated from the different dynamics for PE in isochoric process (Eq. (19) and Eq. (18)). Owing to the different relaxation behavior of PE, the short-time performances of the heat engines also show immense differences.

Another interesting phenomenon is observed for the very short cycle time, $\tau_{\text{cyc}} \ll 1$, where the Lindbladian Otto cycle can work as a heat engine but the Agarwal one cannot. For small τ_{cyc} , we approximate work in Eq. (20) under the condition when the ratios of cycle time to each process time is fixed and $\tau_{\text{ch}} = \tau_{\text{hc}}$ for the simple result.

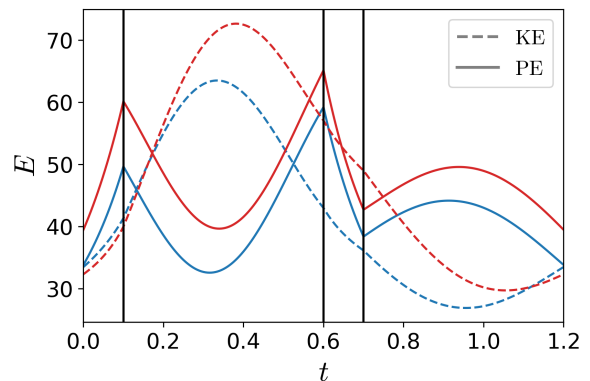


FIG. 4. At $\tau_{\text{cyc}} = 1.2$ when $\eta_{\text{A}} > \eta_{\text{O}}$ (indicated in Fig. 3), the expectation values of the kinetic energy (KE, dashed lines) and the potential energy (PE, solid lines) are plotted as a function of time t , where we set $\tau_{\text{h}} = 0.1$ and $\tau_{\text{hc}} = 0.5$. Three vertical black solid lines represent three boundaries, from the adiabatic compression to the hot isochore, from the hot isochore to the adiabatic expansion, and from the adiabatic expansion to the cold isochore, respectively (from the left to the right). Here we use the same parameters and colors as those used Fig. 3. In Agarwal's adiabatic expansion (the last part for $0.7 \leq t \leq 1.2$, see two blue lines), the PE is always larger than the KE, different from the Lindbladian where the sign of Lagrangian changes. This implies that the friction term, $-\frac{\dot{\omega}(t)}{\omega(t)}\langle\hat{L}\rangle$ in Eq. (13), contributes to $\eta^{\text{A}} > \eta_{\text{O}}$.

The first-order expressions of work are as follows:

$$\begin{aligned} \mathcal{W}^{\text{A}} &= 0 + \mathcal{O}(\tau_{\text{cyc}}^3), \\ \mathcal{W}^{\text{L}} &= \frac{\gamma\tau_{\text{c}}\tau_{\text{h}}(w_{\text{h}}^2 - w_{\text{c}}^2)(\tilde{T}_{\text{h}}w_{\text{c}}^2 - \tilde{T}_{\text{c}}w_{\text{h}}^2)}{4w_{\text{c}}^2w_{\text{h}}^2(\tau_{\text{c}} + \tau_{\text{h}})} + \mathcal{O}(\tau_{\text{cyc}}^2). \end{aligned} \quad (25)$$

Using Eq. (25), the efficiency and power values of two engines are calculated as well. For the Agarwal Otto engine, it is found that $\eta^{\text{A}}, P^{\text{A}} \rightarrow 0$ because $Q_{\text{h}}^{\text{A}} = \frac{\gamma\tau_{\text{c}}\tau_{\text{h}}(\tilde{T}_{\text{c}} - \tilde{T}_{\text{h}})}{4(\tau_{\text{c}} + \tau_{\text{h}})}$ and the first-order term of \mathcal{W}^{A} is zero. So the Agarwal Otto cycle cannot be a heat engine in the short-time limit, which is true even when $\tau_{\text{ch}} \neq \tau_{\text{hc}}$. For the Lindbladian Otto engine, \mathcal{W}^{L} is linearly proportional to τ_{cyc} , so that $P^{\text{L}}, \eta^{\text{L}}$ are non-zero finite and positive when $\omega_{\text{c}}/\omega_{\text{h}} > (\tilde{T}_{\text{c}}/\tilde{T}_{\text{h}})^{1/2}$, which are shown in Fig. 3 as black dashed lines for the Lindblad case. We do not write down the expressions for η^{L} and Q_{h}^{L} , because the expressions are lengthy and complicated.

In the high temperature (classical) limit, such a condition becomes $\omega_{\text{c}}/\omega_{\text{h}} > (T_{\text{c}}/T_{\text{h}})^2$ as plotted in Fig. 5 with blue curved lines. So the valid parameter region in finite-time Otto cycles gets smaller than that in the quasi-static limit case ($\omega_{\text{c}}/\omega_{\text{h}} > T_{\text{c}}/T_{\text{h}}$), which is drawn by orange diagonal lines as guide to the eye in Fig. 5.

Figure 5 shows wavy patterns because of resonance phenomena, which are the same as Fig. 2. and insets correspond to η^k in the quasi-static limit. It is noted that

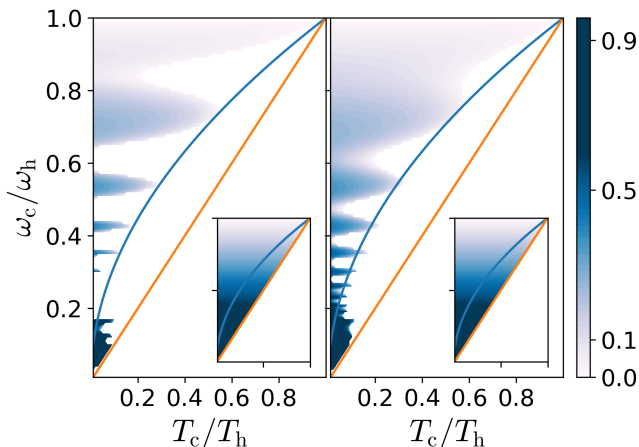


FIG. 5. The contour plots of η^A (left) and η^L (right) are shown as a function of T_c/T_h (temperature ratio, x-axis) and ω_c/ω_h (frequency ratio, y-axis). Here most parameters are the same as before, but we change $\omega_c = 3, T_c = 100, \tau_c = \tau_h = 2$ and $\tau_{ch} = \tau_{hc} = 0.4$, which nicely show how our enumeration result are bounded by the condition derived in high-temperature limit. Blue (orange) guided lines are the boundaries between heat engine and the others such as refrigerator and useless machine in the short-time (quasi-static) limit. The short-time limit was obtained from the Lindbladian work expression of Eq. (25) in high-temperature limit. When the frequency of the harmonic oscillator gets higher, the approximation of the short-time limit cannot be valid anymore. Therefore, $\eta^{A/L}$ near the small frequency ratio can be in-between blue lines and orange ones. The insets correspond to the quasi-static limit, where both cases show the same results.

blue lines are derived from the Lindbladian case, but they quite fit well to the Agarwal case, too. This implies that the adiabatic process strongly relates to the boundary condition rather than the isochore. When the frequency of the working fluid is high, the short-time approximation ($\tau < \omega^{-1}, \gamma^{-1}$) fails, so that data points can exist over blue lines.

IV. CONCLUSION

In summary, we investigated the role of friction in quantum Otto engines with different types of equilibrium heat baths, the Agarwal Otto engine versus the Lindblad Otto engine. In the isochore, their master equations governing the dynamics are different. With the adjoint master equation for the Wigner function, for the second moments, they were exactly derived to solve the performances of the engines exactly with a specific protocol.

Based on our exact derivation of the resonance condition for both engines, we found that the Agarwal Otto engine can exceed the quasi-static Otto efficiency in finite time. This is remarkably different from the Lindblad Otto engine near the resonance condition with odd phase differences, which is also counterintuitive because there is a positive feedback caused by friction. Moreover, in the short cycle-time limit ($\tau_{cyc} \rightarrow 0$), we were also able to derive the approximated expressions of work, which showed that the Lindbladian can have non-zero power, unlike Agarwal Otto engine. It is because the Lindblad bath can directly transfer energy to potential energy, so that the Otto cycle can directly extract energy from potential energy in the short-time limit. Finally, in the finite-time mode, the power of the Lindblad engine is higher than that of the Agarwal engine, and its non-divergent parameter region is larger than the Agarwal engine's. Such differences are originated from the existence of the positional heat channel, which alters the relaxation behavior of potential energy.

Since our results showed that the higher efficiency than the Otto efficiency with non-zero power can be achieved without a special bath, such as squeezed bath, coherent bath or bath with effective negative temperature, we believe that our study could provide some comprehensive picture for better understanding the behavior of fully quantum finite-time Otto engine and suggests how to improve the efficiency of a quantum engine with equilibrium bath of positive temperature in the presence of friction.

ACKNOWLEDGMENTS

This research was supported by Basic Science Research Program through the National Research Foundation of Korea (NRF) (KR) [Grants NRF-2017R1D1A3A03000578 (S.L.,M.H.) and No. NRF-2017R1A2B3006930 (S.L., H.J.)].

[1] J. Gemmer, M. Michel, and G. Mahler, *Quantum Thermodynamics* (Springer-Verlag, Berlin, 2009).
 [2] R. Kosloff and A. Levy, *Annu. Rev. Phys. Chem.* **65**, 365 (2014).
 [3] J. Roßnagel, S. T. Dawkins, K. N. Tolazzi, O. Abah, E. Lutz, F. Schmidt-Kaler, and K. Singer, *Science* **352**, 325 (2016).

[4] M. Josefsson, A. Svilans, A. M. Burke, E. A. Hoffmann, S. Fahlvik, C. Thelander, M. Leijnse, and H. Linke, *Nat. Nanotechnol.* **13**, 920 (2018).
 [5] R. J. de Assis, T. M. de Mendonça, C. J. Villas-Boas, A. M. de Souza, R. S. Sarthour, I. S. Oliveira, and N. G. de Almeida, *Phys. Rev. Lett.* **122**, 240602 (2019).
 [6] R. Uzdin, A. Levy, and R. Kosloff, *Phys. Rev. X* **5**,

- 031044 (2015).
- [7] P. A. Camati, J. F. G. Santos, and R. M. Serra, *Phys. Rev. A* **99**, 062103 (2019).
- [8] T. Guff, S. Daryanoosh, B. Q. Baragiola, and A. Gilchrist, *Phys. Rev. E* **100**, 032129 (2019).
- [9] J. Roßnagel, O. Abah, F. Schmidt-Kaler, K. Singer, and E. Lutz, *Phys. Rev. Lett.* **112**, 030602 (2014).
- [10] Y.-H. Ma, S.-H. Su, and C.-P. Sun, *Phys. Rev. E* **96**, 022143 (2017).
- [11] M. Kloc, P. Cejnar, and G. Schaller, *Phys. Rev. E* **100**, 042126 (2019).
- [12] N. Shiraishi, K. Saito, and H. Tasaki, *Phys. Rev. Lett.* **117**, 190601 (2016).
- [13] P. Pietzonka and U. Seifert, *Phys. Rev. Lett.* **120**, 190602 (2018).
- [14] O. Abah and M. Paternostro, *Phys. Rev. E* **99**, 022110 (2019).
- [15] T. Feldmann and R. Kosloff, *Phys. Rev. E* **68**, 016101 (2003).
- [16] Y. Rezek and R. Kosloff, *New J. of Phys.* **8**, 83 (2006).
- [17] X. Chen, A. Ruschhaupt, S. Schmidt, A. del Campo, D. Guéry-Odelin, and J. G. Muga, *Phys. Rev. Lett.* **104**, 063002 (2010).
- [18] A. Alecce, F. Galve, N. L. Gullo, L. Dell'Anna, F. Plastina, and R. Zambrini, *New J. Phys.* **17**, 075007 (2015).
- [19] Y. Zheng and D. Poletti, *Phys. Rev. E* **90**, 012145 (2014).
- [20] O. Abah, J. Roßnagel, G. Jacob, S. Deffner, F. Schmidt-Kaler, K. Singer, and E. Lutz, *Phys. Rev. Lett.* **109**, 203006 (2012).
- [21] O. Abah and E. Lutz, *EPL* **106**, 20001 (2014); *EPL* **113**, 60002 (2016).
- [22] W. Niedenzu, D. Gelbwaser-Klimovsky, A. G. Kofman, and G. Kurizki, *New J. Phys.* **18**, 083012 (2016).
- [23] J.-M. Park, S. Lee, H.-M. Chun, and J. D. Noh, *Phys. Rev. E* **100**, 012148 (2019).
- [24] P. P. Hofer, J. B. Brask, M. Perarnau-Llobet, and N. Brunner, *Phys. Rev. Lett.* **119**, 090603 (2017).
- [25] A. Insinga, B. Andresen, and P. Salamon, *Phys. Rev. E* **94**, 012119 (2016).
- [26] G. S. Agarwal, *Phys. Rev. A* **2**, 2038 (1970); *Phys. Rev. A* **4**, 739 (1971).
- [27] G. S. Agarwal and S. Chaturvedi, *Phys. Rev. E* **88**, 012130 (2013).
- [28] A. Caldeira and A. Leggett, *Ann. Phys.* **149**, 374 (1983).
- [29] H.-P. Breuer and F. Petruccione, *The Theory of Open Quantum Systems* (Oxford University Press, New York, 2002).
- [30] V. Romero-Rochín, *Phys. Rev. Lett.* **94**, 130601 (2005).
- [31] C. Gardiner and P. Zoller, *Quantum Noise: A Handbook of Markovian and Non-Markovian Quantum Stochastic Methods with Applications to Quantum Optics* (Springer-Verlag, Berlin, 2004).
- [32] H. Risken, *The Fokker-Planck Equation: Methods of Solutions and Applications* (Springer-Verlag, Berlin, 1991).
- [33] J. P. Santos, G. T. Landi, and M. Paternostro, *Phys. Rev. Lett.* **118**, 220601 (2017).
- [34] A. Insinga, B. Andresen, P. Salamon, and R. Kosloff, *Phys. Rev. E* **97**, 062153 (2018).